Transient waves: Reconstruction and processing

J. V. Candy, R. W. Ziolkowski,[a] and D. Kent Lewis
University of California, Lawrence Livermore National Laboratory, P.O. Box 5504, L-156, Livermore, California 94550

(Received 6 April 1990; accepted for publication 27 July 1990)

New solutions to the wave equation have been shown to exhibit enhanced localization and energy fluence characteristics. The transmission and reception of these localized waves create unique problems, since they are essentially transient wave fronts in *both* time and space. Nonetheless, the ability to transmit wave energy through space with these interesting properties has many potential applications in a variety of applications areas. To realize their potential, new methods must be developed to analyze and process these waves. In this paper, approaches to design receiving arrays to reconstruct these special transient waves from noisy measurement data are discussed.

PACS numbers: 43.60.Gk, 43.30.Wi

INTRODUCTION

The propagation of spatiotemporal acoustic signals in water, for instance, is characterized by wave-type phenomenology satisfying the scalar wave equation. Recently, interest has been kindled into the possibility of transmitting wave energy in nonstandard manners. This has resulted from the discovery of pulses and their superpositions that exhibit enhanced localization and energy fluence characteristics.[1-6] The design of arrays to receive these space-time pulses is the subject of this paper—from a signal processing perspective.

We call a pulse with these enhanced localization and energy fluence characteristics a *localized wave* (LW). It has been demonstrated that LW solutions are possible in many real physical systems[3-5] and that the fields launched by driving arrays with these LW pulses exhibit these enhanced localization and energy fluence characteristics.[3,6-8] This LW effect has been confirmed experimentally with an ultrasonic array in water.[7,8]

In terms of transmitting arrays, typical continuous wave (cw) driven apertures use various types of phasing schemes to achieve focusing and beamforming. On the other hand, the LW pulse driven arrays require independently addressable elements—different time signals are launched from different spatial positions in the array. The result is a spatially weighted set of spectra that creates a moving space-time interference pattern that moves away from the array. These LW pulse driven arrays have a vast number of potential applications including microscopes and telescopes with extremely high depths of field, low-loss power transmission, secure communications, remote sensing, and directed energy weapons which explains the wide range of military and industrial interest. However, to realize the potential of this technology, one must be able to receive these signals as well as transmit them. This leads to a large class of new signal processing issues that we will begin to address below.

To simplify the discussion, we will be concerned only with a specific class of the LW solutions to the scalar wave equation—the so-called modified power spectrum (MPS) pulse. This also limits the direct impact of our results primarily to acoustic wave propagation. Analogous vector wave considerations are necessary to achieve similar results for electromagnetic arrays and fields. Our goal is to design sampling arrays capable of reconstructing the MPS pulse from noisy measurement data. This problem is complicated because this pulse is a transient in both time and space leading to a broadband response in both the spatial and temporal frequency domains. First, we will analyze the properties of this pulse that will be useful in limiting the class of arrays to be investigated. This will be discussed in Sec. I. In Sec. II, we will investigate various candidate array designs based on properties of the LW signals and evaluate their performance in reconstruction. We will include information on their performance in the noisy case as well. We will summarize our findings and make suggestions for future research efforts in Sec. III.

I. LOCALIZED WAVES

The pioneering work of Brittingham[1] first suggested the possibility of LW solutions of Maxwell's equations. His original "focus wave modes" represent Gaussian beams that translate through space with only local deformations. They are obtained in a straightforward fashion[2] by assuming a particular form of solution:

$$\Phi_k(x,y,z,t) = e^{ik(z+ct)}G(x,y,z-ct) \tag{1}$$

of the scalar wave equation in real space:

$$\frac{\partial^2}{\partial x^2}\Phi_k(x,y,z,t) + \frac{\partial^2}{\partial y^2}\Phi_k(x,y,z,t) + \frac{\partial^2}{\partial z^2}\Phi_k(x,y,z,t) - \frac{1}{c^2}\frac{\partial^2}{\partial t^2}\Phi_k(x,y,z,t) = 0. \tag{2}$$

This *ansatz* reduces the wave equation to a Schrödinger equation in the pulse center variable $\tau = z - ct$. Introducing the transverse distance $\rho = \sqrt{x^2 + y^2}$, the resulting Schrödinger equation has the solution

$$G(\rho,\tau) = e^{-k\rho^2/(z_0 + i\tau)}/4\pi i(z_0 + i\tau). \tag{3}$$

Thus the original wave equation (2) has

[a] Present address: Dept. of Elec. and Computer Eng., Univ. of Arizona, Tuscon, AZ 85721.

 0001-4966/90/112248-11$00.80

$$\Phi_k(\rho,z,t) = e^{ik(z+ct)} \frac{e^{-k\rho^2/[z_0 + i(z-ct)]}}{4\pi i[z_0 + i(z-ct)]} \tag{4}$$

as an *exact* solution. This pulse has the corresponding parameters: beam spread $A = z_0 + \tau^2/z_0$, phase front curvature $R = \tau + z_0^2/\tau$, and beam waist $w = (A/k)^{1/2}$. This fundamental pulse describes a Gaussian beam that translates through space-time with only local variations. Note that this solution has introduced an added degree of freedom through the variable k that can be exploited. For low values of k, the fundamental Gaussian pulses look like plane waves. Moreover, for all k they share with plane waves the property of having infinite energy. As shown in Ref. 2, these fundamental Gaussian pulse fields can be used as basis functions to represent new transient solutions of the wave equation. The general acoustic LW solution

$$f(\rho,z,t) = \int_0^\infty \Phi_k(\rho,z,t)F(k)dk = \frac{1}{4\pi i[z_0 + i(z-ct)]} \int_0^\infty dk\, F(k)e^{-ks(\rho,z,t)}, \tag{5}$$

where

$$s(\rho,z,t) = \rho^2/[z_0 + i(z-ct)] - i(z+ct) \tag{6}$$

is an exact source-free solution of the wave equation. This representation, in contrast to plane-wave decompositions, utilizes basis functions that are more localized in space and hence, by their very nature, are better suited to describe the directed transfer of acoustic energy in space. The resulting pulses have finite energy if, for example, $F(k)/\sqrt{(k)}$ is square integrable.

Clearly, different spectra $F(k)$ in Eq. (5) lead to different solutions of the scalar wave equation. With a Hertz potential formulation one can adapt those fields to solutions of Maxwell's equations.[3] Many interesting solutions of the wave equation are created simply by referring to a Laplace transform table. One particularly interesting spectrum selection is the modified power spectrum:

$$F(k) = \begin{cases} 4\pi i\beta \dfrac{(\beta k - b)^{\alpha-1} e^{-a(\beta k - b)}}{\Gamma(\alpha)}, & k > \dfrac{b}{\beta}, \\ 0, & 0 \leqslant k < \dfrac{b}{\beta}. \end{cases} \tag{7}$$

It is so called because it is derived from the power spectrum $F(k) = k^{\alpha-1}e^{-ak}$ by a scaling and a truncation. This choice of spectrum leads to the modified power spectrum (MPS) pulse:

$$f(\rho,z,t) = \frac{1}{z_0 + i(z-ct)} \frac{1}{(s/\beta + a)^\alpha} e^{-bs/\beta}. \tag{8}$$

[For the rest of this paper the MPS pulse, $f(\rho,z,t)$, will refer to the real part of Eq. (8) and the direction of propagation will be taken along the positive z axis.] Much effort has been concentrated on this MPS pulse because it has an appealing analytical form and its pulse shape can be tailored to a particular application with a straightforward change in parameters. This transverse behavior of this MPS pulse at the pulse center is essentially

$$f(\rho,z)|_{z=ct} \sim e^{-b\rho^2/\beta z_0} f(\rho,z)|_{\rho=0,z=ct}. \tag{9}$$

The corresponding transverse spatial spectra, that is, the $k_x - k_y$ spectrum at various distances $z = ct$, have been shown numerically to remain nearly invariant as the MPS pulse propagates. Along the direction of propagation z and away from the pulse center the MPS pulse decays as $f \sim 1/[z_0^2 + (z-ct)^2]$. Hence, it is localized along the direction of propagation as well.

Next, we analyze the properties of LW from a signal processing perspective. We investigate the temporal spectra of the MPS pulse, first at the peak of the temporal response. This point corresponds to the maximum of the response within the Gaussian, central portion of the pulse. Second, we will deal with the minimum or tail-dominant part.

We first categorize the overall spectral analysis of the MPS pulse as viewed through a finite linear aperture whose diameter is 2.5 m. We choose a line array of 101 elements spaced 1 cm apart in order to provide enough spatial resolution to observe the major features of the MPS pulse as well as its spectral content. A simulation using Eq. (8) was performed at a spatial-temporal sampling interval ($\Delta\rho = 0.01$ m, $\Delta t = 1\,\mu$s, $z = 0$) with the results shown in Fig. 1. In Fig. 1(a) we see the MPS pulse, $f(\rho,z,t)|_{z=0}$, observed through the 2.5-m linear aperture. Note that this finite aperture truncates the tails of the MPS pulse. This phenomenon is also observed in Fig. 1(b). Here, we see the Gaussian-like pulse (center) and plane wave-like tails. The wave number-frequency spectral domain also reveals some interesting properties in Fig. 1(c) and (d). We again observe a Gaussian-like portion of the spectrum (center) in conjection with low-amplitude tails. We also note that the overall spectrum is bounded by the rectangle [$\pm 20\,\mathrm{m}^{-1}$, ± 5 MHz] with 3-dB bandwidth of [$\pm 2\,\mathrm{m}^{-1}$, ± 0.5 MHz]. Thus we see that the MPS pulse is broadband both temporally and spatially.

Next, we categorize the specific spatiotemporal properties of the MPS pulse. In particular, the MPS pulse is composed of different time signals at different spatial locations. Thus we should select sample time (space) series at representative spatial positions and analyze their particular properties. We have chosen the "maximum" and "minimum" pulse signals in both space and time and have observed their contributions to the overall spectrum. The maximum signal corresponds to the spatial component MPS time signal at which the maximum amplitude is achieved, while the minimum corresponds to the signal in the tail region where the amplitudes are the smallest ones sampled by the array. The results are shown in Fig. 2. In Fig. 2(a) the pulses that are maximum both spatially and temporally are given along with their associated spectra. The latter confirm the 3-dB bandwidth of the 2-D wave number-frequency spectrum. In Fig. 2(b) the pulses that are minimum signals both spatially and temporally are given along with their associated spectra. Both the temporal and spatial spectra appear bandpass in structure with the temporal bandwidth of about 1.0 MHz and center frequency of 1.5 MHz, while the spatial spectrum indicates a bandwidth of $1.5\,\mathrm{m}^{-1}$ with a center frequency of $4.0\,\mathrm{m}^{-1}$. Further examination of the tail-snapshots closer to the Gaussian-like center pulse reveals similar bandpass

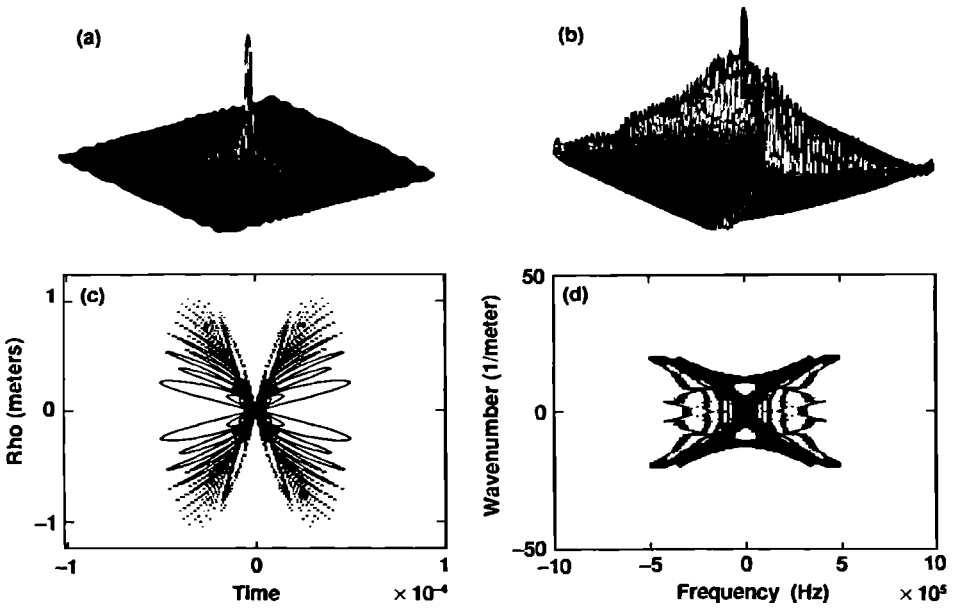

FIG. 1. MPS pulse spectra: (a) Space-time MPS pulse. (b) Space-time MPS pulse contour. (c) MPS frequency-wave number spectrum. (d) MPS frequency-wave number contour.

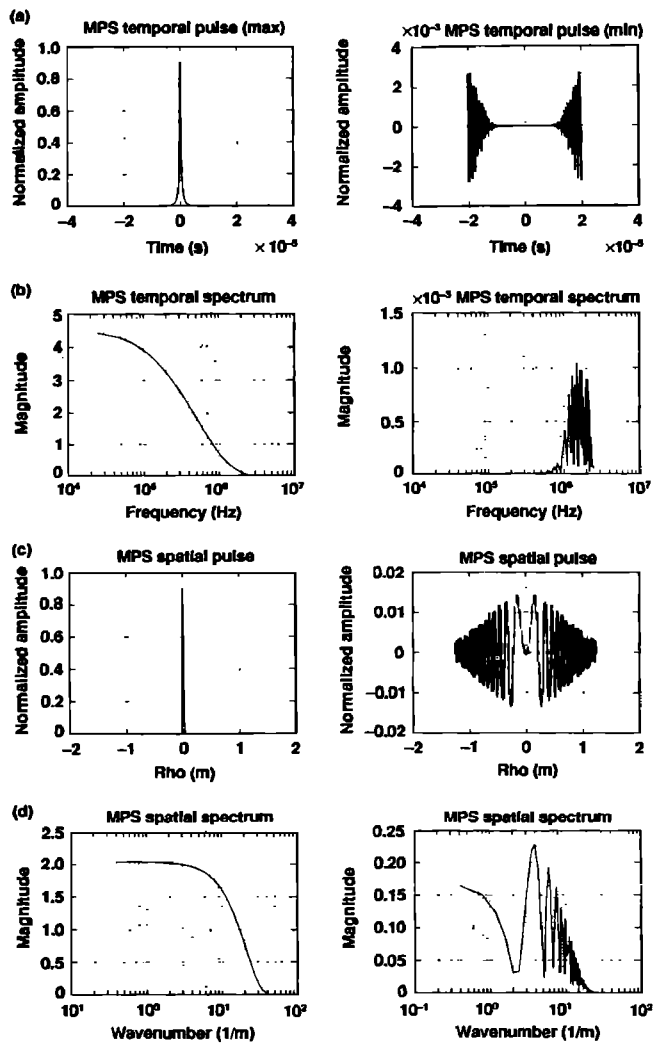

FIG. 2. MPS maximum and minimum pulse signals: (a) Maximum temporal and spatial signals and spectra. (b) Minimum temporal and spatial signals and spectra.

structure with varying center frequencies and bandwidths. We summarize these properties of the MPS pulse in Table I.

Next we analyze the correlation properties of the LW solutions assuming a purely random (white) noise field. In particular, we define a random function, say f, as a one-dimensional, time-varying, random field in three-dimensional Euclidean space and time such that $f(x,y,z,t) = f(\underline{\rho},t)$. The corresponding *spatiotemporal correlation* function is defined by

$$R_{ff}(\underline{\rho},\tilde{\underline{\rho}},t,\tilde{t}) := E\{f(\underline{\rho},t)f^*(\tilde{\underline{\rho}},\tilde{t})\}, \tag{10}$$

where $\{\cdot\}$ is the expectation value over all space-time. For small spatial distances or aperture sizes we make the assumption of wide-sense stationarity and homogeneity.[9] This leads to simplifications that

$$R_{ff}(\underline{\rho},\tilde{\underline{\rho}},t,\tilde{t}) = R_{ff}(\underline{\xi},\tau) := E\{f(\underline{\rho},t)f^*(\underline{\rho}+\underline{\xi},t+\tau)\}, \tag{11}$$

where $\tau = t - \tilde{t}$ and $\underline{\xi} = \underline{\rho} - \tilde{\underline{\rho}}$. Thus the spatiotemporal correlation function in the stationary case is a function between two points and only depends on the time and space differences between them. Note that for homogeneous and stationary processes the Wiener–Khintchine theorem holds; and we have the corresponding power spectrum defined by the Fourier transform pair (continuous or discrete):

$$\begin{aligned} P_{ff}(\kappa,f) &:= F[R_{ff}(\underline{\xi},\tau)], \\ R_{ff}(\underline{\xi},\tau) &= F^{-1}[P_{ff}(\kappa,f)], \end{aligned} \tag{12}$$

for κ, f the respective wave number and temporal frequencies.

If the spatially and temporally sampled wave is observed through a discrete 2-D array, then $\rho \to \rho_l$ and $f(\underline{\rho},z,t_k) \to f(\underline{\rho}_l,z,t_k)$. Thus the corresponding spatiotemporal correlation function is given by $R_{ff}(\underline{\rho}_l,\tilde{\underline{\rho}}_l,t_k,\tilde{t}_k)$ and in the stationary case by $R_{ff}(\underline{\xi}_l,m)$.

TABLE I. MPS pulse characteristics: $a = 1$ m, $b = 600\ \mathrm{m}^{-1}$, $\alpha = 1$, $\beta = 300$, $z_0 = 4.5\times10^{-4}$ m, $c = 1500$ m/s.

Characteristic		Theory (Infinite aperture) Boundary	Amplitude	Simulation (2.5-m aperture) Max	Min
Near zone	$(z<\beta/2b)$	<0.25 m	$f=1$ (constant)	same	same
Intermediate zone	$(z\sim\beta/2b)$	~0.25 m	$0<f<1$ (period $= n\pi/4$)	same	same
Far zone	$(z>\beta a/2)$	>150 m	$f<1/150$ $(1/z)$	same	same
Amplitude decay (@ $1/e$)	$(\rho = /\beta z_0/b)$	0.15 m	$f=1/e$	0.04 m	
Waist (@ 150 m)	$(\omega = \beta z_0/b)$	1.5 cm	···	···	
Temporal center frequency	(F_0)	0.27 MHz	···	0.2 MHz	1.5 MHz
Temporal 3-dB bandwidth	(F_{low})	0.5 MHz	···	0.2 MHz	1.0 MHz
Highest temporal frequency	(F_{high})	0.53 MHz	···	0.2MHz	2.2 MHz
Lowest temporal frequency	(F_{low})	478 Hz	···	0	1.2 MHz
Spatial center frequency	(κ_0)	0.32(1/m)	···	12(1/m)	4.0(1/m)
Spatial 3-dB bandwidth	(κ_{low})	0.32(1/m)	···	12(1/m)	1.5(1/m)
Highest spatial frequency	$(\kappa_{\mathrm{high}}$	0.32(1/m)	···	12(1/m)	4.5(1/m)
Lowest spatial frequency	(κ_{low})	357(1/m)	···		3.0(1/m)
Highest wavelength	$(\lambda_{\mathrm{high}})$	3.14 m	···	0.083	0.33 m
Lowest wavelength	(λ_{low})	2.8×10^{-3} m	···	···	0.22 m
Highest Nyquist sampling	(d_{high})	1.57 m	···	0.04 m	0.17 m
Lowest Nyquist sampling	(d_{low})	1.42×10^{-3} m	···	···	0.11 m

In order to estimate this spatial correlation function *at each snapshot* t_k, we use the estimator

$$\hat{R}_{ff}(\underline{\xi},t_k) = \frac{1}{N(\underline{\xi})}\sum_{l=1}^{N(\underline{\xi})} f(\underline{\rho}_l,z,t_k)f(\underline{\rho}_l+\underline{\xi},z,t_k), \quad (13)$$

where $N(\underline{\xi})$ is the number of sensor pairs separated by the distance vector $\underline{\xi}$. If we constrain the arrays to be uniform, then the spatial correlation function can be estimated using fast Fourier transform techniques. Additionally, Eq. (12) holds true. With these estimators and concepts in mind, we will now analyze some of the spatial properties of the MPS pulse.

We have used apertures larger in size than one would use in practice for a given MPS pulse to allow for a complete characterization of the corresponding spatial correlations and spectra. The MPS truth pulse is again observed through a uniformly spaced line array of 101 sensors but here with a 1.0-m-diam aperture. The space-time wave at $z = 0$ for 101 temporal samples at a uniform interval of $\Delta t = 0.2$ μs is shown in Fig. 3(a). Since the line array is uniformly spaced, we can use 2-D Fourier transform techniques to estimate the spatiotemporal correlation function $\hat{R}_{ff}(\underline{\xi},\tau)$ and the corresponding wave number-frequency spectrum $\hat{P}_{ff}(\underline{\kappa},f)$. The results for this case are shown in Fig. 3(b). As expected, most of the correlated transient energy of the MPS pulse (passing through this aperture) is concentrated in the Gaussian pulse region. In particular, the correlations lie primarily between $\xi = \pm 0.1$ m [see contours in Fig. 3(c)] with the corresponding wave number-frequency spectrum lying between [$\pm 20\ \mathrm{m}^{-1}$, 0.5 MHz]. Recall that the waist of this MPS pulse is 0.015m. These results are similar to those obtained previously for the deterministic MPS pulse and spectrum.

To design an array to receive an LW signal such as the MPS pulse, we must determine primarily its spatial frequency content over the spatial extent of the array. We analyze the spatial spectrum exclusively by estimating the spatial correlation *at a given snapshot in time*, that is, we estimate $\hat{R}_{ff}(\underline{\xi},t_k)$ and $\hat{P}_{ff}(\underline{\kappa},t_k)$ at each snapshot t_k. The results of the spatial estimation for the line array are shown in Fig. 4. Both the spatial correlation and the energy spectrum at each snapshot are displayed. Note that most of the correlated energy is again concentrated within ± 0.1 m, which represents the Gaussian center region of the MPS pulse for broadside incidence. Sensors placed outside this region will tend to sample the MPS tails. The corresponding wave number spectrum indicates that most of the spectral energy is bounded in wave number below $\pm 20\ \mathrm{m}^{-1}$.

This completes the discussion on the analyses of the spatiotemporal properties of the MPS pulse. In the next section we will illustrate how these properties can be used to design various arrays to receive LW pulses.

II. SAMPLING ARRAY DESIGN

A. Design constraints

The design of an array to receive a localized wave is a difficult problem because of its spatially dependent, transient nature. One can view this problem as one of designing a spatial filter to pass certain frequencies and rejecting others. However, as the analysis of the previous section showed, the frequency wave number spectrum of the MPS pulse is quite complex and varies at each position.

One approach might be to select a sensor arrangement producing a spatial pattern with enough spatial bandwidth to pass the desired pulse and then weight it at each time snapshot with the actual function. This means take $f(\rho_l,z,t_k) = f(\rho,z,t)|_{\rho=\rho_l,t=t_k}$ so that at each snapshot t_k the weight at location ρ_l is, in fact, $f(\rho_l,z,t_k)$. Thus at the next time instant t_{k+1}, the weight becomes $f(\rho_l,z,t_{k+1})$. Unfortunately, for this scheme to function properly, the pulse must be precisely aligned and its onset detected.

In this section, we will consider a more conservative approach, the design of spatial filters for certain bandwidths. We will introduce the concept and the design of *sampling*

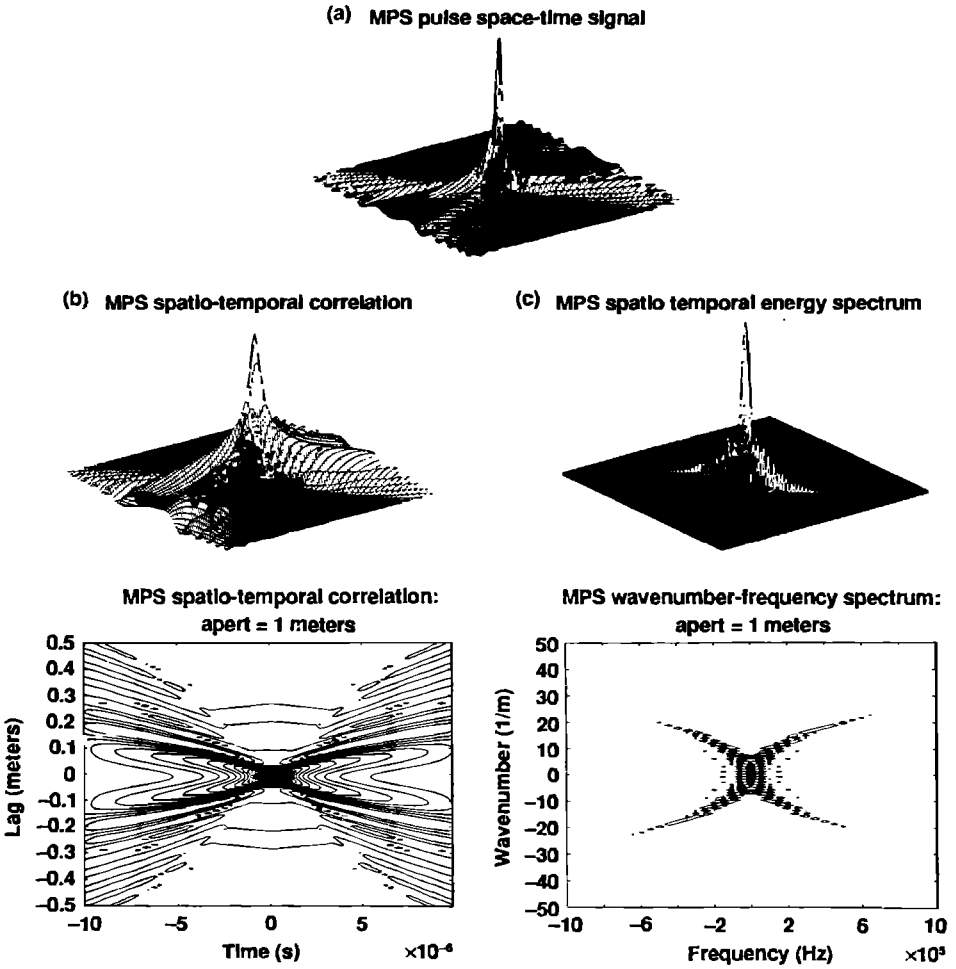

FIG. 3. MPS pulse correlation/spectrum for $L = 101$ element line array with 1-cm spacing: (a) Space-time pulse for 1-m aperture. (b) Spatio-temporal correlation. (c) wave number-frequency energy spectrum.

arrays to distinguish them (in principle) from the typical designs of narrow-band antenna arrays for plane or spherical wave fronts. [In this paper, we are concerned with the spatial sampling of the MPS pulse for reconstruction purposes.] As stated previously, our main goal is to investigate designs that can be used for the reception of localized waves.

The constraints on sampling array designs for localized waves are based on the property that they minimize spatial aliasing and enable reconstruction of the LW at the receiver. We limit our discussion to designs specifically for the MPS pulse. Recall the following properties of the MPS pulse that will affect our design: (1) transient wave (nonplanar wave front); (2) broadband spatiotemporal spectrum ([± 20 m^{-1}, ± 0.5 MHz]); and (3) circularly symmetric wave function [$f(x,y,z,t) = f(\rho,z,t)$].

From our previous analysis of the MPS pulse at $z = 0$, we noted that the temporal frequency response appears low pass with its 3-dB cutoff located near 0.5 MHz. Typically, we expect to observe this pulse through a receiving array somewhere along the axis of propagation. Therefore, selection of $z = 0$ as a spatial position to investigate is not a good choice. Through analysis it has been shown[7] that the temporal spectrum of the MPS pulse is bandpass with low- and high-cutoff frequencies of $f_{\text{low}} = bc/2\pi\beta = 477.5$ Hz and $f_{\text{high}} = c/2\pi z_0 = 0.53$ MHz. In water, we have a propagation velocity of $c = 1500$ m/s; hence, the corresponding wavelengths ($\lambda = c/f$) are: $\lambda_{\text{high}} = 3.14$ m and $\lambda_{\text{low}} = 2.83 \times 10^{-3}$ m. Now, if we translate these wavelengths to Nyquist sampling ($d \leqslant \lambda/2$), then we see that the constraints on the sensor spacing to reconstruct the MPS pulse must be: $d_{\text{high}} \leqslant 1.57$ m and $d_{\text{low}} \leqslant 1.42 \times 10^{-3}$ m. We also note that using this criteria satisfies the Nyquist sampling for both the maximum and minimum pulses since the corresponding wavelengths are: $\lambda_{\text{max}} = 0.083$ m and $\lambda_{\text{min}} = 0.33$ m implying $\lambda_{\text{low}} \leqslant \lambda_{\text{max}} \leqslant \lambda_{\text{min}} \leqslant \lambda_{\text{high}}$. We have summarized all of these properties in Table I.

B. Array design concepts

With these constraints of symmetry and spectra in mind, we have investigated the design of two-dimensional (2-D) sampling arrays situated along the axis of propagation (z axis). Since the MPS pulse is circularly symmetric, sensors placed on different radii emanating from the origin will uniquely sample it. However, in a more practical sense, when noise is present it becomes necessary to have sensor redundancy to help enhance signal-to-noise ratio (SNR). The *sampling array design procedure* we have employed is to

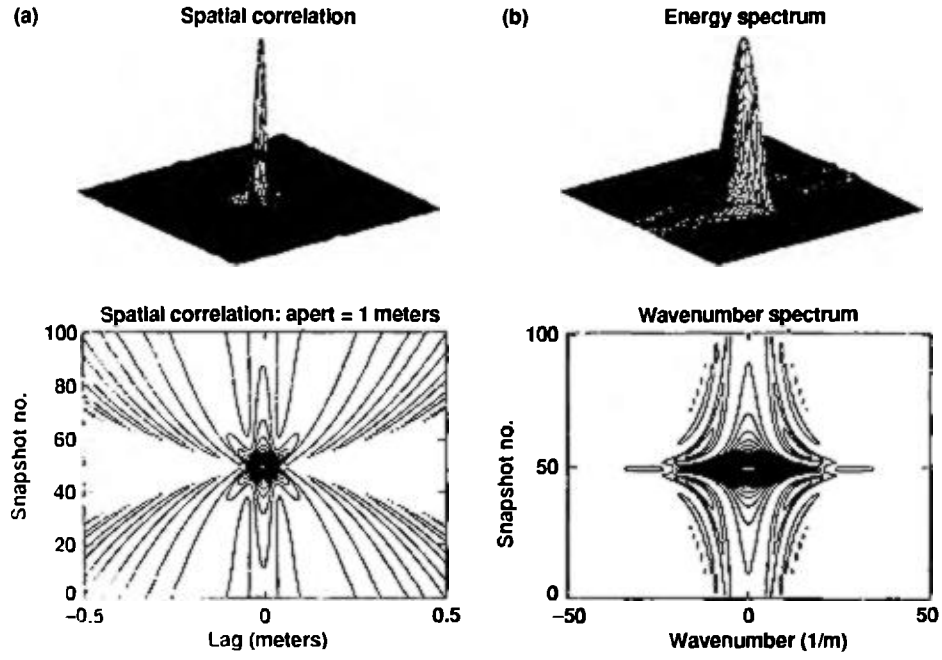

FIG. 4. MPS pulse spatial correlation spectrum for $L = 101$ element line array with 1.0-cm spacing at each snapshot: (a) spatial correlation. (b) wave number energy spectrum.

(1) select the candidate design; (2) determine its spatial bandwidth properties; (3) reconstruct the LW from its spatial samples; and (4) compare the reconstructed LW with the "truth" LW simulated by a line array with identical spacing.

For our reconstruction problem, we simulate the MPS truth pulse using the parameters of Table I with a sampling interval of $\Delta T = 2 \times 10^{-7}$ s and an aperture of $D = 0.1$ m using a line array of $L = 101$ sensors spaced at $d = 0.001$ m apart. The results are shown in Fig. 5. We will use the truth pulse to assess the reconstruction performance.

First, let us consider some "standard" 2-D array designs and analyze their spectral and sampling properties. We will then proceed to some more customized MPS designs. To account for our practical experimental and fabrication capabilities, we constrain the aperture size to $D = 0.1$ m and the number of sensors to $L = 121$.

If we were to select a 2-D planar array design with uniform spatial sampling interval $(\Delta x, \Delta y)$, then the MPS pulse is sampled as

$$f(x_m, y_n, z, t) = f(m\Delta x, n\Delta y, z, t),$$

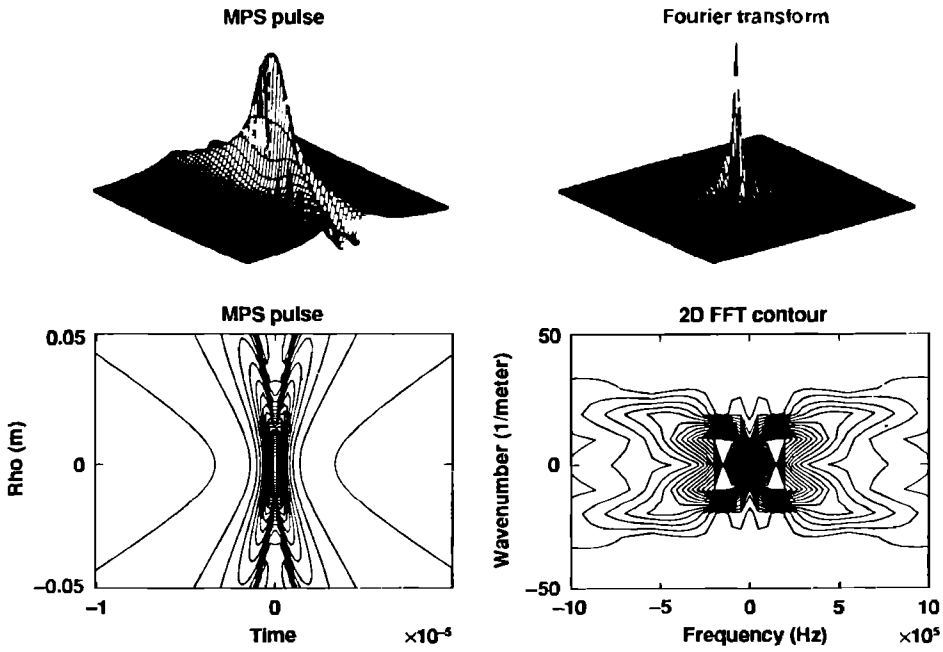

FIG. 5. MPS pulse truth simulation for $L = 101$ element line array with 1.0-mm spacing.

for a general 2-D *rectangular* sampling array of length L. If the sampling is uniform and equal in both x and y, that is, $\Delta x = \Delta y = \Delta$, and if the intersensor spacing d of the largest linear dimension D of the aperture is given by

$$D = (L-1)\Delta, \quad d = \Delta,$$

then the sampling of the signal over the array is

$$f(x_m,y_n,z,t) = f(m\Delta,n\Delta,z,t), \quad m,n = 0,1,...,L-1. \tag{14}$$

In particular, if we were to choose to design an 11×11 square array with $d = 0.01$-m spacing, the associated Nyquist sampling $d \geqslant d_{\text{low}} = 0.0014$ m. Therefore, some spatial aliasing would occur in this case. On the other hand, if we were to use *hexagonal* sampling[13] with the same array size and element spacing, the signal samples

$$f(x_m,y_n,z,t) = f(2m\Delta x + 2n\Delta x, m\Delta y - n\Delta y, z, t).$$

Choosing $\Delta x = \Delta y = \Delta$, we would then have

$$f(x_m,y_n,z,t) = f[2\Delta(m+n), \Delta(m-n), z, t], \quad m,n = 0,1,...,L-1. \tag{15}$$

Both designs satisfy the spatial bandwidth requirement, that is, the passband of $\pm 20\ \text{m}^{-1}$ is satisfied. Another approach is to directly sample in radius (ρ) and place any redundant sensors on circles defined by each radii. The resulting array is called the *coincentric circular* design. In this case we see that the sampled MPS pulse is given by

$$f(\rho_{mn},z,t), \quad m = 0,1,...,N_\rho - 1, \quad n = 0,1,...,L_{m-1}, \tag{16}$$

where N_ρ is the number of distinct radii (circles) and L_m is defined as the number of sensors in the mth circle. Note also that the total number of sensors is given by

$$\sum_{m=0}^{N_\rho - 1} L_m = L.$$

In the case of a deterministic signal (noise free), one has

$$f(\rho_{mn},z,t) = f(\rho_{m0},z,t) = \cdots = f(\rho_{mL_m-1},z,t).$$

This indicates the redundancy available in the coincentric circular design that will be exploited in signal processing to increase the SNR in a noisy environment.

These square, hexagonal, and coincentric circular arrays possess reasonable patterns to pass much of the MPS energy. However, the MPS pulse is very broadband; and we must investigate designs that exhibit even broader response patterns.

Arrays that theoretically have no bandwidth limitation are called frequency independent. The low-frequency limit is determined by the size of the array while the high-frequency limit is bounded by the precision in fabrication. One of these frequency independent designs is the log-periodic array. It is so named because it has a response that is periodic with the logarithm of the frequency. A variation of our coincentric circular design is the *log-periodic coincentric circular* array. The elements in this array are located in positions whose radii are selected according to the following function[14]

$$\rho_m = \rho_0 \alpha^m, \quad m = 0,1,...,N_\rho - 1, \tag{17}$$

where ρ_0 is the minimum required Nyquist spacing, N_ρ is the number of distinct radii (circles), and

$$\alpha = (2\rho_{N_\rho}/\rho_0)^{1/N_\rho}.$$

The distance ρ_{N_ρ} is the half-aperture length ($D/2$). It has been shown (see Followill[10]) that it is desirable to select an odd number of sensors per circle starting with a sensor at the origin and increasing the number of sensors per circle until the total number available are utilized. For our $L = 121$ element design, the resulting log-periodic coincentric circular pattern is shown in Fig. 6(a). Again note that we maintain the redundancy properties of the coincentric design, but obtain a much broader pattern.

Our final design is also considered to be frequency independent. It is the so-called *log-spiral* array. In this design we distribute the sensors in the array logarithmically on a spiral with the initial sensor location at ρ_0 (above) based on the minimum Nyquist spacing and the largest ρ_L determined by the maximum allowable aperture dimension D. The equations for this design are given by

$$\rho_m = e^{b\phi_m}, \quad m = 0,1,...,L-1, \tag{18}$$

with

$$\phi_m = \ln \rho_0/b + (m-1)\Delta\phi,$$

and

$$\Delta\phi = [1/(L-1)]\ln(\rho_L/\rho_0),$$

where ρ is the radius from the spiral origin to the sensor. The terms ρ_0 and ρ_L are bounding circles of the array defining (according to the Nyquist sampling constraints) its minimum and maximum radii, respectively. The constant b is the spiral rate constant: $b = (1/\rho)(d\rho/d\phi)$.

Note that this log-spiral design offers some desirable features based on the MPS properties. Besides the broadband response shown by the pattern in Fig. 6(b), it enables "unique" sampling of the MPS pulse. This sampling property is very useful in a high SNR environment. Many sensors are located around the origin providing a large number of samples of the Gaussian-like center portion of the pulse whereas fewer sensors are located along the array extremities to sample the low-frequency MPS tails.

C. Array sampling properties

Having completed the discussion of the various candidate designs selected, we now consider the capability of these

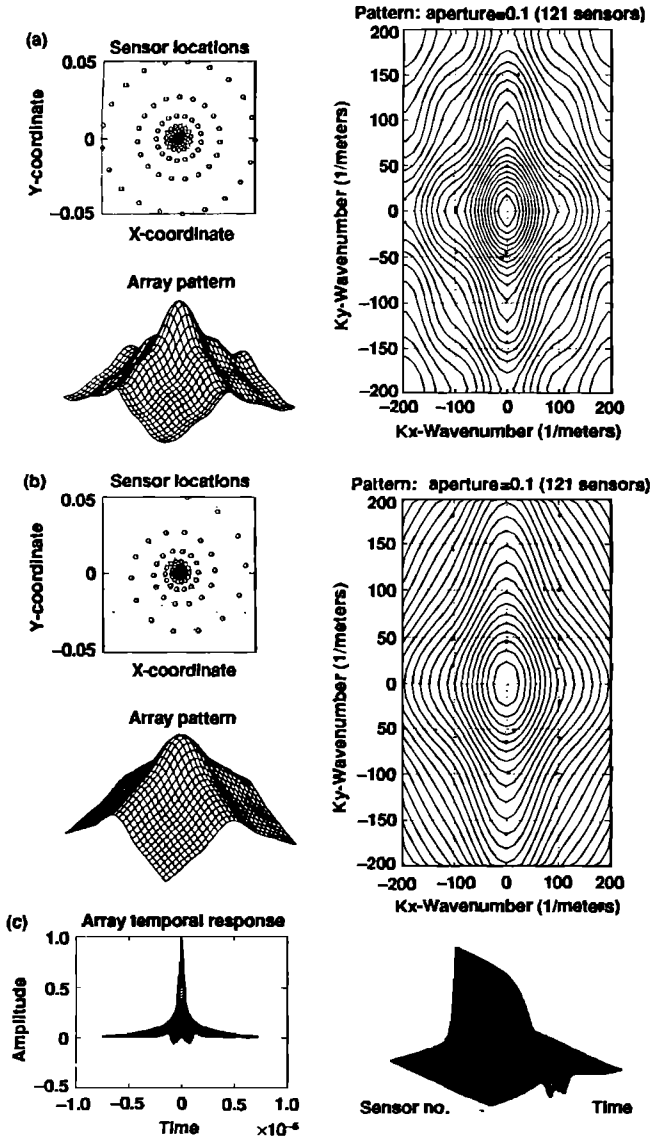

FIG. 6. MPS pulse array design: (a) Log-periodic circular array and pattern. (b) Log spiral array and pattern. (c) MPS pulse sampling using log spiral array.

arrays to reconstruct the MPS pulse from simulated data. Since most of the arrays selected have some design redundancies, it will only be necessary to use the unique (in radius) samples for reconstruction. In particular, since the MPS pulse is circularly symmetric, any 2-D sampling array will satisfy the relation

$$f(x_m,y_n,z,t) = f(\rho_{mn},z,t), \quad m = 0,...,L_x - 1, \quad n = 0,...,L_y - 1, \tag{19}$$

and

$$\rho_{mn} = \sqrt{x_m^2 + y_n^2}, \quad m = 0,...L_x - 1, \quad n = 0,...,L_y - 1,$$

where the total number of sensors

$$L = L_x \times L_y.$$

For given sets of sensor coordinates $(\{x_m\},\{y_n\})$ we then have

$$\rho_{mn} = \rho_{ij}, \quad \text{for } \{x_m\},\{y_n\} \quad \forall m,n \in I_{ij}.$$

Mathematically, this means that all redundant sensors at locations $(\{x_m\},\{y_n\})$ lie in the index set, I_{ij} of unique sensors having the same radius ρ_{ij}. From a sampling and reconstruction point of view, we are only interested in the unique samples of the MPS pulse. Therefore, we only require the set of unique radii $\{\rho_{ij}\}$ for reconstruction. Thus in effect we are actually constructing a 1-D line array perpendicular to the axis of propagation with enough spatial bandwidth to uniquely sample the MPS pulse in ρ. Note that we are no longer uniformly sampling this function. For instance, consider the square array shown in Fig. 7. In Fig. 7(a) the full square array, including redundant sensors and the corresponding sampled MPS function, are shown. The redundant sensors result in bands of time signals that are identical. Extraction of the unique samples from the array (neglecting the symmetrical portion of the function) leads to the results shown in Fig. 7(b). It illustrates the nonuniform spacing of the sensors (displayed on a line at 0) and the corresponding signals. Note that of the 121 sensors in the square array only 20 provide unique spatial samples in radius. In contrast to the square array, the log-spiral design is shown in Fig. 6(c). All 121 sensor signals are given because each sensor in that design provides a unique sample of the MPS pulse. Moreover, it has a large number of samples of the Gaussian-like center portion of the MPS pulse. In contrast, the square array samples the tails more densely.

The other arrays discussed above yield similar results. In particular, the number of unique samples provided by each array is: log spiral (121), square (20), hexagonal (15), log-periodic circular (11), and coincentric circular (11). Next we must consider the reconstruction problem using these arrays.

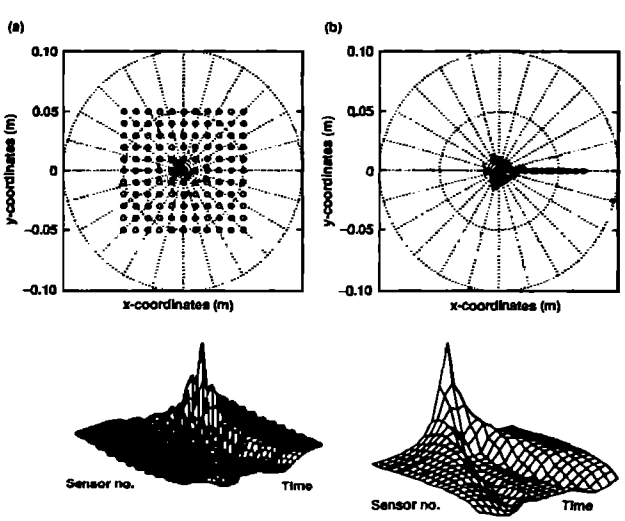

FIG. 7. MPS pulse sampling with the square array: (a) redundant sampling. (b) Unique (radius) sampling.

D. LW reconstructions

The problem of reconstructing the MPS pulse from a set of discrete spatial samples is the prime motivation in designing the sampling arrays. More formally, we would like to determine an $\hat{f}(\rho,z,t)$ such that the *reconstruction error*

$$\epsilon(\rho,z,t) = f(\rho,z,t) - \hat{f}(\rho,z,t)|_{\rho=\rho_{mn}}$$

is minimized. In the ideal case, the signal (according to the sampling theorem) is "exactly" reconstructed from its sampled values using cardinal interpolation (see Candy[11]) as long as Nyquist sampling can be achieved. Unfortunately, this solution requires an infinite aperture or a spatially band-limited signal, neither condition being satisfied by the theoretical MPS case under consideration.

Our reconstruction approach is to develop a 1-D spatial interpolation that sorts through available samples for the preselected interval and linearly interpolates between missing samples. A linear interpolator to obtain uniform spatial samples (temporal sampling is already uniform) is given by

$$\hat{f}(\rho,z,t) = f(\rho_l,z,t_k), \quad l=0,\ldots,N_\rho-1, \quad k=0,\ldots,N_t-1. \tag{20}$$

[Here, we always assume that any 2-D array design has been "resampled" to remove sensor redundancies providing N_ρ unique spatial samples.]

For fixed z,t_k the interpolator is defined by

$$\hat{f}_l(i) := f[\rho_l(i),z,t_k].$$

Explicitly, the linear algorithm is: select $\Delta\rho(i)$, then

$$\rho_l(i+1) = \rho_l(i) + \Delta\rho(i), \tag{21}$$

$$\hat{f}_l(i+1) = \hat{f}_l(i) + \left(\frac{\Delta f_l}{\Delta\rho_l}\right)\rho_l(i+1), \quad i=0,\ldots,N_l-1,$$

where

$$\Delta f_l = f(\rho_l,z,t) - f(\rho_{l-1},z,t),$$
$$\Delta\rho_l = \rho_l - \rho_{l-1},$$
$$N_l = \Delta\rho_l/\Delta\rho(i),$$

and

$$f_l(0) = f(\rho_{l-1},z,t), \quad f_l(N_l) = f(\rho_l,z,t),$$
$$\rho_l(0) = \rho_{l-1}, \quad \rho_l(N_l) = \rho_l.$$

In this scheme, a desired spatial sampling interval $\Delta\rho(i)$ is preselected over the entire aperture length. Those samples coinciding with this sampling criterion are used directly; the samples missing those points are linearly interpolated. In this way we achieve a *uniformly* sampled spatial-temporal function from the nonuniform array samples given by

$$\hat{f}[\rho(i),z,t_k], \quad i=0,\ldots,N_\rho-1; \quad k=0,\ldots,N_t-1. \tag{22}$$

The corresponding wave number-frequency spectrum at a given distance away from the array z is estimated using the 2-D Fourier transform, that is,

$$F[\kappa_\rho(m),\Omega_t(n),z] = \sum_{i=0}^{N_\rho-1}\sum_{k=0}^{N_t-1}\hat{f}[\rho(i),z,t_k]\,e^{-j[\kappa_\rho(m)i+\Omega_t(n)k]}, \tag{23}$$

where $\kappa_\rho(m) := (2\pi/N_\rho)m$ and $\Omega_t(n) := (2\pi/N_t)n$. Some of the reconstructions and corresponding spectra are shown in Figs. 8 and 9. Statistically, we can quantify the reconstruction error by its mean and root-mean square given by

$$m_\epsilon(\rho,r,t) = E[\epsilon(\rho,z,t)],$$
$$\epsilon = \sqrt{E[\epsilon(\rho,z,t)^2] - \{E[\epsilon(\rho,z,t)]\}^2}. \tag{24}$$

These terms are estimated using the usual statistical sampling techniques. The error is calculated by comparing the reconstructed pulse to the "truth" pulse generated at the same spatial sampling interval used by the interpolator.

A typical reconstruction estimate for the square array is shown in Fig. 8. Here, we see the reconstructed MPS pulse. Comparing with the truth pulse in Fig. 5, we note the similarity in structure. Observing the error surface and the corresponding Fourier spectrum, we first note that the majority of the error for the square array occurs in the reconstruction of the Gaussian-like portion of the MPS pulse. This is located at the center of the error contour in Fig. 8(c) and corresponds to the high frequencies of the wave-number spectrum contour. In contrast to this square array reconstruction, we observe the log-spiral array results in Fig. 9. As expected, since the log spiral has many unique spatial samples of the Gaussian-like portion of the MPS pulse, most of the associated reconstruction error is located in the tail regions. This is illustrated by the error contour in Fig. 9(c) at the upper and lower parts of the figure. The corresponding error spectrum

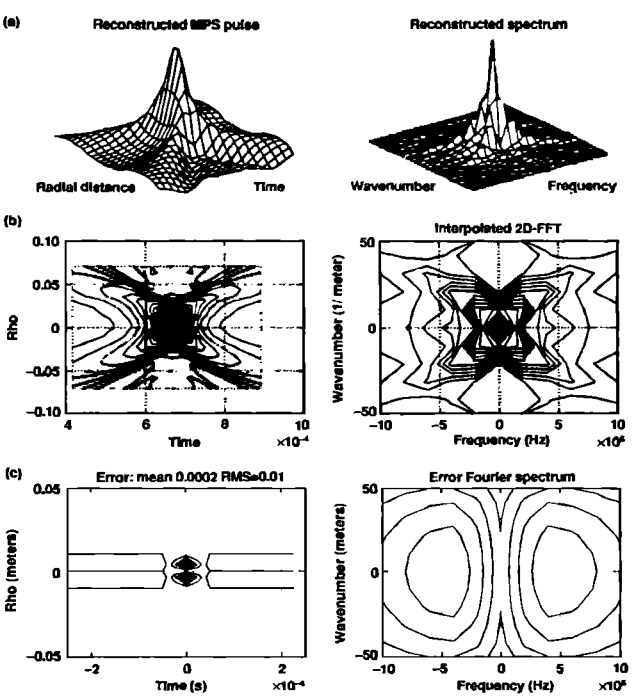

FIG. 8. MPS pulse reconstruction from a square sampling array. (a) Reconstructed MPS pulse and corresponding 2-D Fourier spectrum. (b) Pulse and spectral contours. (c) Error and error spectrum contours.

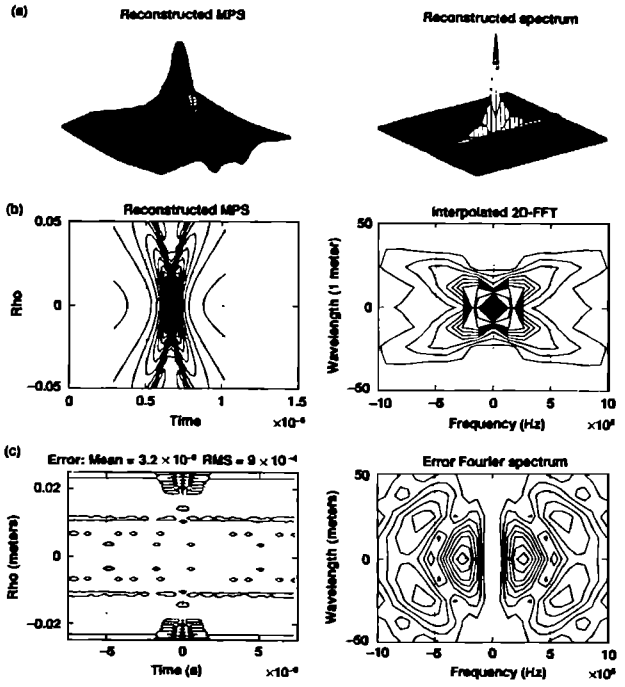

FIG. 9. MPS pulse reconstruction from a log-spiral sampling array. (a) Reconstructed MPS pulse and corresponding 2-D Fourier spectrum. (b) Pulse and spectral contours. (c) Error and error spectrum contours.

indicates that most of the error energy occupies the lower frequency part of the wave-number spectrum (see Fig. 9). Statistically, the mean and rms reconstruction error statistics indicate superior performance by the log-spiral array over the square array, since m_ϵ:$(3\times10^{-6}<200\times10^{-6})$ and σ_ϵ:$(8.5\times10^{-4}<95\times10^{-4})$.

When noise is present, however, it is necessary to perform some signal processing to achieve satisfactory performance. For instance, observe in Fig. 10 the performance of the square array when additive Gaussian noise is introduced at 45 dB SNR. The noisy measured MPS pulse is defined by

$$y(\rho_{mn},z,t_k)=f(\rho_{mn},z,t_k)+v(\rho_{mm},z,t_k), \tag{25}$$

for

$$m=0,...,L_x-1,\quad n=0,...,L_y-1,\quad k=0,...,N_t-1,$$

where y is the field measured at sensor location (x_m,y_n) corresponding to radius ρ_{mn} at z and time (snapshot) t_k; f is the deterministic but unknown LW function spatially sampled at ρ_{mn}; and v is the zero-mean, Gaussian random noise field with covariance R_{vv}.

The signal-to-noise ratio is then defined by: SNR: $=$ (peak)$^2/\sigma_v^2$. Clearly, the reconstruction has severely deteriorated when noise is present.

The redundant sensors in the array designs can be used to achieve an improvement to overall SNR. If we perform *signal averaging* spatially over the redundancies, then the processed signal is given by

$$\hat{f}(\rho_l,z,t_k)=\frac{1}{L_xL_y}\sum_{m=0}^{L_x-1}\sum_{n=0}^{L_y-1}y(\rho_{mn},z,t_k),$$
$$k=0,...,N_t-1,\ l=0,...N_\rho-1. \tag{26}$$

Recall that N_ρ is the number of unique spatial samples (in radii). After processing, the reconstruction is performed as before using the interpolator. The results for the square array are also shown in Fig. 10(c) for comparison with the deterministic simulations of Fig. 8. More sophisticated interpolator designs can be achieved using the actual model [Eq. (8)] to predict between samples, but these represent work for the future.

III. SUMMARY

Various designs of arrays to sample and reconstruct transient waves from noisy measurement data have been developed. Particular applications of these sampling array designs were applied to LW pulse reconstruction in noiseless and noisy environments. Using properties of the particular wave function under investigation, it has been shown that log-periodic designs coupled with a spatial interpolation scheme can satisfactorily reconstruct the desired wave. When noise is present, it was shown that redundant sensors can be used to improve the SNR and therefore array performance. Future work will investigate coupling the advantages of both design concepts into distinct sets of subarrays

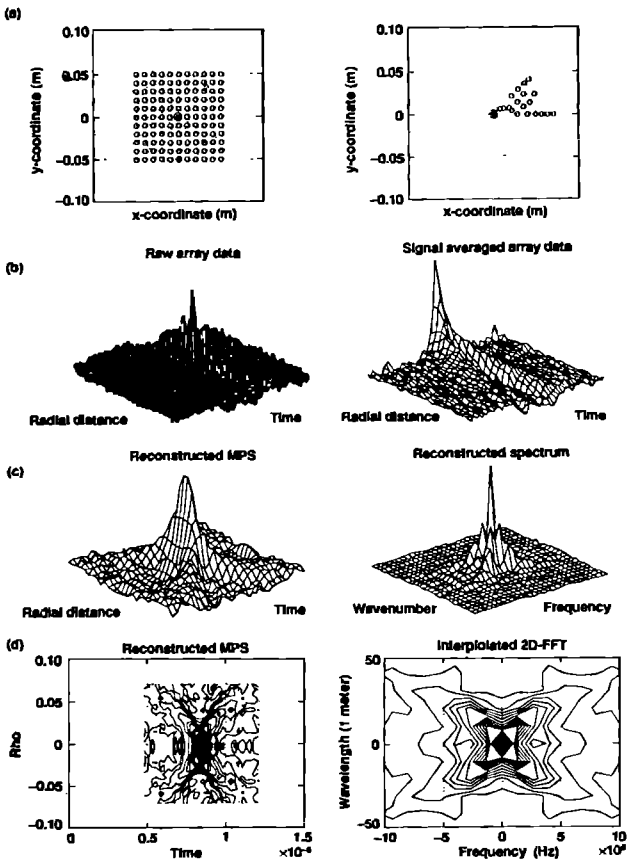

FIG. 10. MPS pulse reconstruction from a square sampling array of noisy measurement data (SNR = 45 dB) using signal averaging. (a) Array and 2-D unique sensor sampling. (b) Total measured and signal average data. (c) Reconstruction and 2-D Fourier spectrum. (d) Reconstructed (interpolated) signal and spectral contours.

in a larger array thereby achieving the optimum performance. We will also try to demonstrate that improved performance can be attained by using interpolators incorporating the wave model[12] into the reconstruction process even in a noisy environment.

[1] J. B. Brittingham, "Focus wave modes in homogeneous Maxwell's equations: transverse electric mode," J. Appl. Phys. **54**, 1179–1189 (1983).

[2] R. W. Ziolkowski, "Exact solutions of the wave equation with complex source locations," J. Math. Phys. **26**(4), 861–863 (1985).

[3] R. W. Ziolkowski, "Localized transmission of electromagnetic energy," Phys. Rev. A **39**(4), 2005–2033 (1989).

[4] A. M. Shaarawi, I. M. Besieris, and R. W. Ziolkowski, "Localized energy pulse train launched from an open, semi-infinite circular waveguide," J. Appl. Phys. **65**(2), 805–813 (1989).

[5] I. M. Besieris, A. M. Shaarawi, and R. W. Ziolkowski, "A bidirectional travelling plane representation of exact solutions of the scalar wave equation," J. Math. Phys. **30**(6), 1254–1269 (1989).

[6] E. Heyman and L. B. Felsen, "Spectral analysis of focus wave modes," J. Opt. Soc. Am. A **6**(6), 806–813 (1989).

[7] R. W. Ziolkowski, D. K. Lewis, and B. D. Cook, "Evidence of localized wave transmission," Phys. Rev. Lett. **62**(2), 147–150 (1989).

[8] R. W. Ziolkowski and D. K. Lewis, "Verification of the localized wave transmission effect," to be published in J. Appl. Phys. (1991).

[9] A. Baggeroer, "Space/Time Random Processes and Optimum Array Processing," Naval Undersea Center Rep., NUC TP 506, 1976.

[10] F. Followill, Lawr. Lurmv. Nat. Lab., personal communication, 1989.

[11] J. V. Candy, *Signal Processing: The Modern Approach* (McGraw-Hill, New York, 1988).

[12] J. V. Candy, *Signal Processing: The Model-Based Approach* (McGraw-Hill, New York, 1986).

[13] D. E. Dundgeon and R. M. Mersereau, *Multidimensional Digital Signal Processing* (Prentice-Hall, Englewood Cliffs, NJ, 1984).

[14] Y. T. Lo and S. W. Lee, *Antenna Handbook: Theory, Applications and Design* (Van Nostrand Reinhold, New York, 1988).